

Quantum Beating Patterns Observed in the Energetics of Pb Film Nanostructures

P. Czoschke,^{1,2} Hawoong Hong,² L. Basile,^{1,2} and T.-C. Chiang^{1,2}

¹*Department of Physics, University of Illinois at Urbana-Champaign, 1110 W. Green Street, Urbana, Illinois 61801-3080, USA*

²*Frederick Seitz Materials Research Laboratory, University of Illinois at Urbana-Champaign, 104 S. Goodwin Avenue, Urbana, Illinois 61801-2902, USA*

(Received 5 March 2004; published 16 July 2004)

We have studied the nanoscale structural evolution of Pb films grown at 110 K on a Si(111) substrate as they are annealed to increasingly higher temperatures. Surface x-ray diffraction from a synchrotron source is used to observe the morphology evolve from an initial smooth film through various metastable states before reaching a state of local equilibrium, at which point the coverage of different height Pb structures is analyzed and related to the thickness-dependent surface energy. Rich patterns are seen in the resulting energy landscape similar to the beating patterns heard from the interference of two musical notes of similar pitch. The explanation is, however, very simple, as demonstrated by a model calculation based on the confinement of free electrons to a quantum well.

DOI: 10.1103/PhysRevLett.93.036103

PACS numbers: 68.35.Md, 61.10.Kw, 68.55.Jk, 68.65.Fg

The fast approach of technological devices to sizes comparable with their atomic constituents makes a fundamental understanding of how such nanoscale structures behave in this realm of utmost importance. For instance, electronic contributions have been shown to play a vital role in the stabilization of various metallic nanoscale structures, including atomically uniform films [1–3] and uniform height self-organized islands [4–8]. Such electronic effects can be calculated from first principles [9,10], but obtaining empirical information about the general energy landscape and the electronic contributions thereto with which to compare such theoretical calculations is experimentally difficult. The technique of x-ray diffraction is well equipped to provide such information experimentally for thin film nanostructures. It measures absolute thicknesses as opposed to surface properties as it is with electron-diffraction and scanned-probe techniques, and it provides a statistical sampling over a large macroscopic area of the sample, eliminating any questions about statistical significance that are often present in microscopy studies. With the thickness distribution of an ultrathin film determined after annealing to attain local equilibrium, one can deduce the relative thermodynamic stability of different island heights from which details of the surface energy can be determined. We have used x rays from a synchrotron source to carry out diffraction studies of epitaxial Pb nanostructures grown on a Si(111) substrate that reveal details of the functional form of the surface energy over a wide range of thicknesses in the quantum regime. Beating patterns superimposed on rapid oscillations are observed and attributed to quantum confinement effects in agreement with a free-electron model calculation.

To explore the energetics of the system, Pb nanostructures were formed by the thermal evaporation of films of various thicknesses onto a Si(111) substrate prepared in an ultrahigh vacuum chamber custom built for surface

x-ray diffraction at UNICAT (University-National Laboratory-Industry Collaborative Access Team), Advanced Photon Source, Argonne National Laboratory. The samples were prepared by annealing a clean Si(111)-(7 × 7) reconstructed surface with a 4.5 Å Pb overlayer to 415 °C for 10 min. This process produces the $\frac{1}{3}$ -monolayer coverage commensurate Pb/Si(111)-($\sqrt{3} \times \sqrt{3}$)R30°-β reconstructed surface [11,12], which was verified by examining reflection high energy electron diffraction patterns, in-plane x-ray superstructure peaks, and the extended x-ray reflectivity. Pb films were then deposited with the sample held at 110 K at a rate of 0.84 Å/min. Quoted temperatures are the average reading of two thermocouples attached to tantalum mounting clips at both ends of the sample. After deposition, the samples were annealed to temperatures around 280 K by slowly increasing a direct current.

At multiple points during the annealing process, the morphology of the film was examined by quenching the system back to 110 K and scanning the extended x-ray reflectivity. Such data are shown in Fig. 1 for a sample with an initial coverage of 11 atomic layers (AL) of Pb. The data points represent the integrated intensity for perpendicular momentum transfers $l = 3-12$, where l is in Si reciprocal lattice units (1 r.l.u. = 0.668 Å⁻¹), measured by collecting a series of parallel line scans in reciprocal space around the specular condition to achieve both integration and background subtraction. Although data were collected every 5–10 K, only a small subset of the data is shown in Fig. 1 to illustrate the major morphological changes. To fit the data, we constructed a standard kinematic model [13,14], taking into account interference with the substrate, the internal lattice relaxations of the Pb film due to interface-induced Friedel oscillations [15], and a partial coherence factor. The detailed structure of the film (i.e., the relative occupancies of the atomic layers) was determined from the parameters

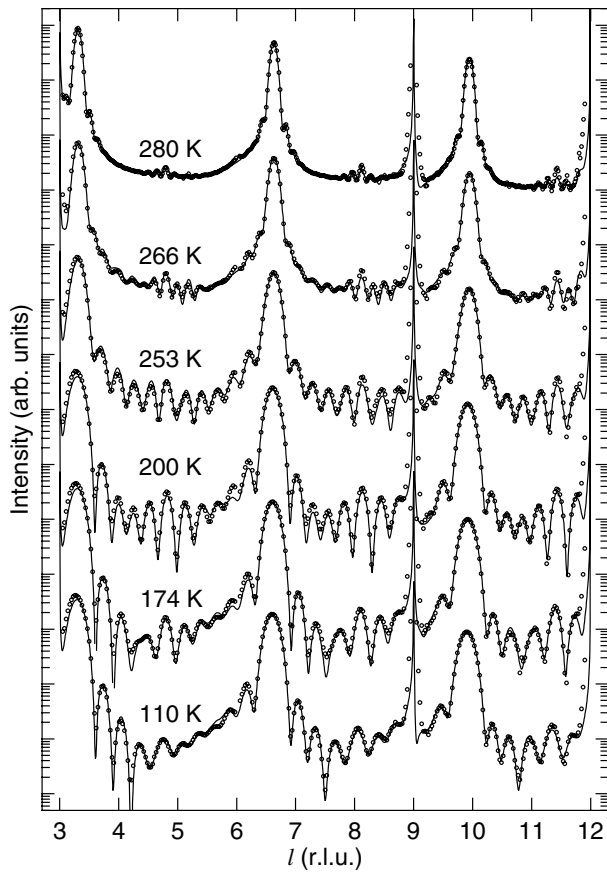


FIG. 1. Extended x-ray reflectivity of a sample with an initial thickness of 11 AL after annealing to the temperatures indicated. Curves are fits that reveal the relative coverage of different film thicknesses present on the sample surface. The sharp peaks at $l = 3, 9,$ and 12 are Bragg peaks from the Si(111) substrate, and the broad peaks at $l \approx 3.3, 6.6,$ and 9.9 are Bragg peaks from the Pb(111) overlayers.

p_N , defined as the fractional surface area that is covered by N atomic layers of Pb, which were ultimately fit as free parameters. The fit for each temperature was started from the best fit of the previous temperature, effectively following the film morphology as the physical system evolved with continued annealing. The uniqueness of the solution was verified by performing multiple fits from different initial conditions and checking that nearly the same solution was obtained (the fractional deviation found was less than 10% of each p_N). The resultant p_N values for each temperature are shown in Fig. 2 for each corresponding curve in Fig. 1.

At low temperatures, the system is known to follow a nearly layer-by-layer growth mode [15]. After film deposition at 110 K (bottom curve in Fig. 2), the surface is covered by a closed film with an average thickness of 11 AL and a very small roughness of 3.2 Å (rms). The next two curves in the figure show that as the film is annealed to 200 K, the film bifurcates into the neighboring thicknesses of 10 and 12 AL, which as will be seen are

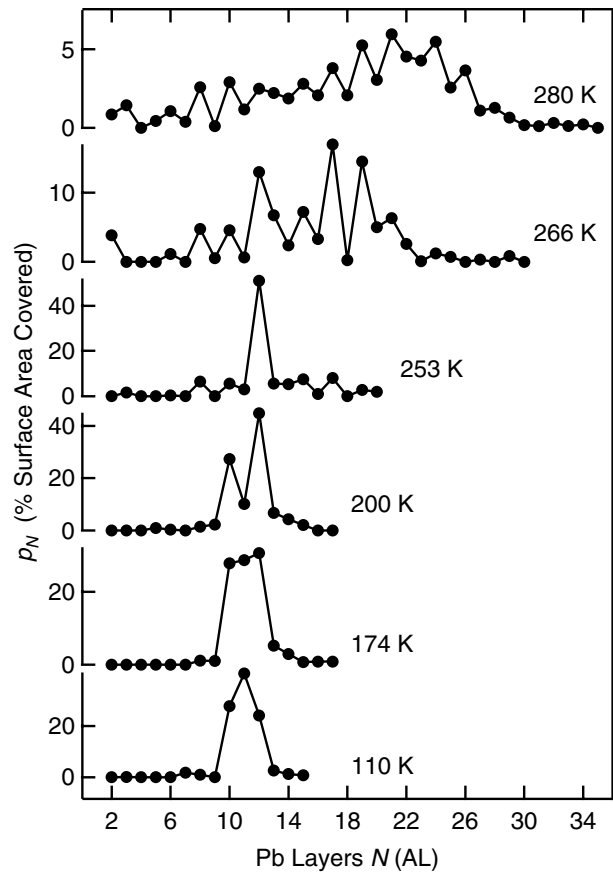


FIG. 2. Coverage of different thicknesses on the surface extracted from fits to each curve in Fig. 1. The surface morphology evolves from an initial thickness of 11 AL, through various “preferred thickness” states, and finally into a state of local equilibrium. Oscillations in the values are readily apparent in the high-temperature states, which correspond to variations in the relative surface energy of the system. Multiple nodal points in these oscillations are also evident at which the preference for even or odd thicknesses changes. These points are due to a longer-wavelength beating pattern in the surface energy.

energetically more favorable than 11 AL. As the temperature increases further to near 250 K, the surface atoms have enough mobility to yield a broader thickness distribution with a single dominating thickness at 12 AL. The system in this range of temperatures is in the metastable “preferred height” phase that reflects mostly the local energy landscape and kinetics near the initial thickness. Since the preferred height is larger than the initial film coverage, the surface morphology consists of uniform-height islands on top of a wetting layer, similar to the nanoislands seen in previous microscopy studies of similar systems [5,6]. At even higher temperatures, the system has enough thermal energy to escape the local energy minimum at the preferred height to explore the broader energy landscape and a corresponding roughening of the film occurs. By 280 K, the preference for 12 AL has disappeared and the film thickness distribution becomes

very broad (rms roughness of 27.7 Å). At this point, the system has presumably reached a state of local equilibrium, in which each particular thickness N is in equilibrium with its neighboring thicknesses, $N \pm 1$. The rapid fluctuationlike variations in p_N , superimposed on the broad distribution, indicate correspondingly rapid variations in the energy landscape.

An experimental measure of the relative stability of each thickness can be obtained by comparing the surface coverage of that thickness with its neighbors:

$$p_N - \frac{p_{N-1} + p_{N+1}}{2} = -\frac{1}{2}p_N'' \quad (1)$$

where p_N'' is the discrete second derivative of p_N . That is, thicknesses for which the local curvature of p_N is negative are relatively stable and correspond to an excess of p_N relative to the local average value based on its neighbors. The quantity p_N'' for the 280 K data in Fig. 2 is shown in Fig. 3(a) as solid circles. Bilayer oscillations are seen indicating an energetic preference for either even or odd film thicknesses, with alternation between the two every 9 AL or so. This effect is analogous to the beating pattern that results from the interference of two sinusoidal functions of similar frequency.

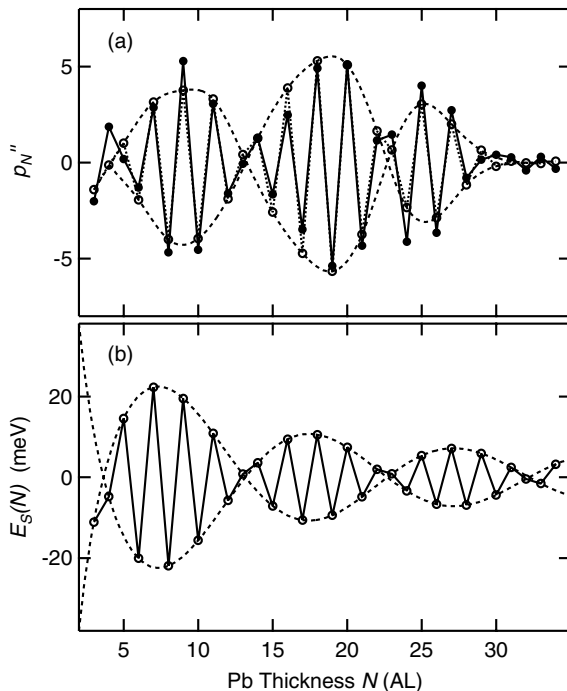


FIG. 3. (a) The discrete second derivative of the 280 K curve in Fig. 2 (filled circles) and a fit to the data (open circles) as described in the text. Lines are guides for the eye. The envelope function for the fit is also shown, highlighting the beating pattern in the oscillations. (b) The corresponding relative surface energy, which also shows the presence of a beating pattern decaying with increasing thickness. This effect arises from the quantization of electronic states in the Pb nanostructures due to quantum confinement.

The beating pattern can be attributed to the effects of quantum confinement of the electrons in the Pb film. The confinement results in a film energy that depends sensitively on the thickness. Since Pb is a simple free-electronlike metal, a model based on a free-electron gas confined to a quantum well should capture the essential physics of the system, including the seemingly complex appearance of the beating pattern. This is indeed the case, as demonstrated below. A straightforward numerical calculation of a quantum well filled with free electrons at the Pb density yields a surface energy that can be well described by the Friedel form

$$E_s(N) = A \frac{\cos[2k_F(N + \Delta N)t_0]}{(N + \Delta N)^\alpha} + B, \quad (2)$$

where $k_F = 1.59 \text{ \AA}^{-1}$ is the Fermi wave vector for Pb(111), $t_0 = 2.84 \text{ \AA}$ is the thickness of each AL, $\alpha = 0.938$, and the parameters A and B are constants. The parameter ΔN is included to account for the fact that the effective width of the quantum well may be slightly larger than Nt_0 due to charge spillage effects [15]. Namely, the Pb film does not have an infinite potential barrier at the boundaries, and the electrons can tunnel outward somewhat. This parameter is equivalent to an adjustable boundary phase shift. Equation (2) describes a damped sinusoidal function with a Friedel oscillation wavelength equal to half the Fermi wavelength [16]. In the present case, it is equal to $\lambda = \pi/k_F = 0.691t_0$. Since the surface energy is sampled at only integer values of N , the oscillations appear to have a period of 3λ , or approximately 2 AL, riding on an envelope “beating” function with an internode distance of $\lambda/(3\lambda - 2) \approx 9 \text{ AL}$.

The connection between p_N and the surface energy should follow a Boltzmann distribution

$$p_N \propto e^{-E_s(N)/k_B T}, \quad (3)$$

where k_B is Boltzmann’s constant and T is the temperature of the system, which is taken to be the annealing temperature. However, the proportionality of Eq. (3) strictly holds only if the system is in a state of global equilibrium. In the present case, we have attained only a state of local equilibrium in which the “constant” of proportionality in Eq. (3) is a slowly varying function of N . To avoid this nonspecific function that depends on the annealing history, we consider instead the self-normalized local variations in p_N :

$$\delta p_N \equiv \frac{p_N - \bar{p}_N}{\bar{p}_N}, \quad (4)$$

where \bar{p}_N is a local average of p_N . δp_N does not depend on the proportionality constant as long as \bar{p}_N is calculated using only a small local set of p_N ’s. Such a local average corresponds to the smoothly varying background underlying the oscillations in the p_N data shown in Fig. 2. A reasonable choice for the local average is to use a binomial filtering algorithm [17],

$$\bar{p}_N = \frac{p_{N-1} + 2p_N + p_{N+1}}{4}, \quad (5)$$

which has the added benefit that δp_N is simply related to the discrete second derivative of p_N

$$\delta p_N = \frac{-p_N''}{4\bar{p}_N}, \quad (6)$$

as discussed in connection with Eq. (1). Calculations of δp_N using Eqs. (2) and (3) were performed to fit the experimental values of p_N'' . There were only two adjustable parameters in the fit, A and ΔN , since the constant B cancels out of δp_N .

Figure 3(a) displays the results of the fit, shown by open circles, to the experimental values of p_N'' , shown by filled circles, using the function

$$(p_N'')_{\text{theory}} = -4(\bar{p}_N)_{\text{expt}}(\delta p_N)_{\text{theory}}, \quad (7)$$

where $(\bar{p}_N)_{\text{expt}}$ is calculated from the experimental data using Eq. (5). The fit reproduces the data remarkably well considering that the model contains only two adjustable parameters, and it clearly captures the oscillatory behavior as well as the proper beating superperiod. The corresponding relative surface energy calculated using Eq. (2) with the fitted parameters (and B set to zero) is shown in Fig. 3(b), which also displays beating patterns with the same nodal points as the experimental data. The fitted value for the charge spillage parameter, $\Delta N = 0.30 \pm 0.02$ corresponds to an expansion of the quantum well by $0.87 \pm 0.06 \text{ \AA}$, a very reasonable value. The overall energy scale of the surface energy curve is also consistent with the results of recent first-principles calculations for related systems [9,10].

In the classical limit, in which the spectrum of allowed electronic states approaches a continuum, the relative surface energy is a constant, with no energetic preference for one thickness over another. However, when confinement of the itinerant electrons in the metallic structure is taken into account, oscillations in the surface energy of the form Eq. (2) arise, leading to a relative preference of certain thicknesses over others. It is seen that a smooth film represents a metastable state which, upon annealing, evolves through preferred or magic structures to a thermodynamically more stable, highly roughened state. X-ray diffraction allows an accurate determination of the statistical distribution of the heights, from which variations in surface energy can be deduced. The beating patterns observed in the data are a direct consequence of this quantum confinement, providing another dramatic example of the importance of quantum effects in the design and properties of metallic nanoscale objects.

This work is supported by the U.S. Department of Energy (Grant No. DEFG02-91ER45439). The UNICAT

facility at the Advanced Photon Source (APS) is supported by the University of Illinois at Urbana-Champaign, Frederick Seitz Materials Research Laboratory (U.S. DOE, and the State of Illinois-IBHE-HECA), the Oak Ridge National Laboratory (U.S. DOE under contract with UT-Battelle LLC), the National Institute of Standards and Technology (U.S. Department of Commerce), and UOP LLC. The APS is supported by the U.S. DOE under Contract No. W-31-109-ENG-38. We also acknowledge partial equipment and personnel support from the Petroleum Research Fund, administered by the American Chemical Society, and the U.S. National Science Foundation (Grant No. DMR-02-03003).

-
- [1] A. R. Smith, K.-J. Chao, Q. Niu, and C.-K. Shih, *Science* **273**, 226 (1996).
 - [2] D.-A. Luh, T. Miller, J. J. Paggel, M. Y. Chou, and T.-C. Chiang, *Science* **292**, 1131 (2001).
 - [3] H. Yu, C. S. Jiang, P. Ebert, X. D. Wang, J. M. White, Q. Niu, Z. Zhang, and C. K. Shih, *Phys. Rev. Lett.* **88**, 016102 (2002).
 - [4] L. Gavioli, K. R. Kimberlin, M. C. Tringides, J. F. Wendelken, and Z. Zhang, *Phys. Rev. Lett.* **82**, 129 (1999).
 - [5] M. Hupalo, V. Yeh, L. Berbil-Bautista, S. Kremmer, E. Abram, and M. C. Tringides, *Phys. Rev. B* **64**, 155307 (2001).
 - [6] W. B. Su, S. H. Chang, W. B. Jian, C. S. Chang, L. J. Chen, and T. T. Tsong, *Phys. Rev. Lett.* **86**, 5116 (2001).
 - [7] A. Mans, J. H. Dil, A. R. H. F. Ettema, and H. H. Weitering, *Phys. Rev. B* **66**, 195410 (2002).
 - [8] R. Otero, A. L. Vázquez de Parga, and R. Miranda, *Phys. Rev. B* **66**, 115401 (2002).
 - [9] C. M. Wei and M. Y. Chou, *Phys. Rev. B* **66**, 233408 (2002).
 - [10] H. Hong, C.-M. Wei, M. Y. Chou, Z. Wu, L. Basile, H. Chen, M. Holt, and T.-C. Chiang, *Phys. Rev. Lett.* **90**, 076104 (2003).
 - [11] J. A. Carlisle, T. Miller, and T.-C. Chiang, *Phys. Rev. B* **45**, 3400 (1992).
 - [12] F. Grey, R. Feidenhans'l, M. Nielsen, and R. L. Johnson, *Colloq. Phys.* **C7**, 181 (1989).
 - [13] I. K. Robinson and D. J. Tweet, *Rep. Prog. Phys.* **55**, 599 (1992).
 - [14] J. Als-Nielsen and D. McMorrow, *Elements of Modern X-Ray Physics* (John Wiley and Sons, Ltd., Chichester, 2001).
 - [15] P. Czoschke, H. Hong, L. Basile, and T.-C. Chiang, *Phys. Rev. Lett.* **91**, 226801 (2003).
 - [16] Z. Zhang, Q. Niu, and C.-K. Shih, *Phys. Rev. Lett.* **80**, 5381 (1998).
 - [17] P. Marchand and L. Marmet, *Rev. Sci. Instrum.* **54**, 1034 (1983).